Supplementary Information

Enhancement of piezoelectricity of [001]-textured (K, Na)(Nb, Sb)O_3-(Bi, Ag)ZrO_3 ceramics using $Na(Nb_{0.9}Sb_{0.1})O_3$ templates at low temperature

*Seung-Hyun Kim, Geun-Soo Lee, Jung-Soo Kim, San Kwak, Byeong-Jae Min, and Sahn Nahm**

Department of Materials Science and Engineering, Korea University, 145 Anam-ro, Seongbuk-gu, Seoul, 02841, Republic of Korea

1. NNS templates and measurement of various physical properties of the ceramics

The NNS templates were produced using molten salt and topochemical methods. Bi_2O_3, Na_2CO_3, Nb_2O_5, and Sb_2O_5 raw powders (≥ 99.9%, High Purity Chemicals, Japan) were used to fabricate the $Bi_{2.5}Na_{3.5}(Nb_{4.5}Sb_{0.5})O_{18}$ [BNNS] precursor. The raw powders with the appropriate ratio were mixed by ball milling for 12 h and heated in molten NaCl (≥ 99.9%, High Purity Chemicals, Japan) at 1150 ℃ for 6 h to produce the BNNS precursor. Furthermore, the NNS templates were produced using the topochemical microcrystal conversion reaction between BNNS precursor and Na_2CO_3 at 975 ℃ for 6 h in molten NaCl. Figure S1(a) shows the X-ray diffraction (XRD) pattern of the NNS templates. A perovskite phase without secondary phases was developed in the NNS templates. The size of the NNS template was approximately 15 μm × 1.0 μm, as shown in Figure S1(b). Therefore, it can be concluded that the NNS templates are well formed.

The crystal structures of the samples were determined using X-ray diffraction (XRD; XRD-6100, Shimadzu, Kyoto, Japan) using Cu *Kα* radiation. The textured ceramics have been crushed into the powders with a size of approximately 0.6 μm for the XRD measurements. XRD patterns of the textured ceramic powders were obtained at a low scan rate (1.0°/min). The XRD patterns of the piezoelectric ceramics were analyzed via Rietveld refinement using the FullProf suite program to determine the detailed crystal structures of the samples. Moreover, the degree of [001] texturing should be considered when XRD patterns are refined using the FullProf suite program. Field-emission scanning electron microscopy (SEM; S-4800, Hitachi, Tokyo, Japan) was used to study the microstructures, and SEM and back scattered SEM (BSEM) images of the samples were obtained. Furthermore, compositional analysis of the samples was performed using energy-dispersive X-ray spectroscopy (EDX; EMAX, Horiba, Japan) integrated with SEM. The densities of the specimens were measured using Archimedes' principle. The piezoceramics were coated with silver electrodes and poled in silicone oil at room temperature (RT) using a DC electric field of 4 kV/mm for 30 min. The piezoelectric charge constants (d_{33}) were measured using a d_{33} meter (ZJ-4B; Academia Sinca, China). Further, dielectric constant ($\varepsilon^T_{33}/\varepsilon_0$) values were measured at various temperatures using an impedance analyzer (HP 4194A, Agilent Technologies, Santa Clara, CA, USA). The heating rate of the ε_r versus temperature curves is approximately 1.0 ^oC/min. The [001]-textured and untextured $CKN(N_{0.95}S_{0.05})$-BAZ piezoceramics were used to produce the cantilever-shaped

piezoelectric energy harvesters (C-PEHs). The [001]-textured piezoceramic plates (15 mm × 15 mm × 0.4 mm) were attached to the steel substrates (SUS304) with the size of 15 mm × 60 mm × 0.4 mm using DP-420 epoxy. A schematic of the C-PEH is shown in Figure S1(c).

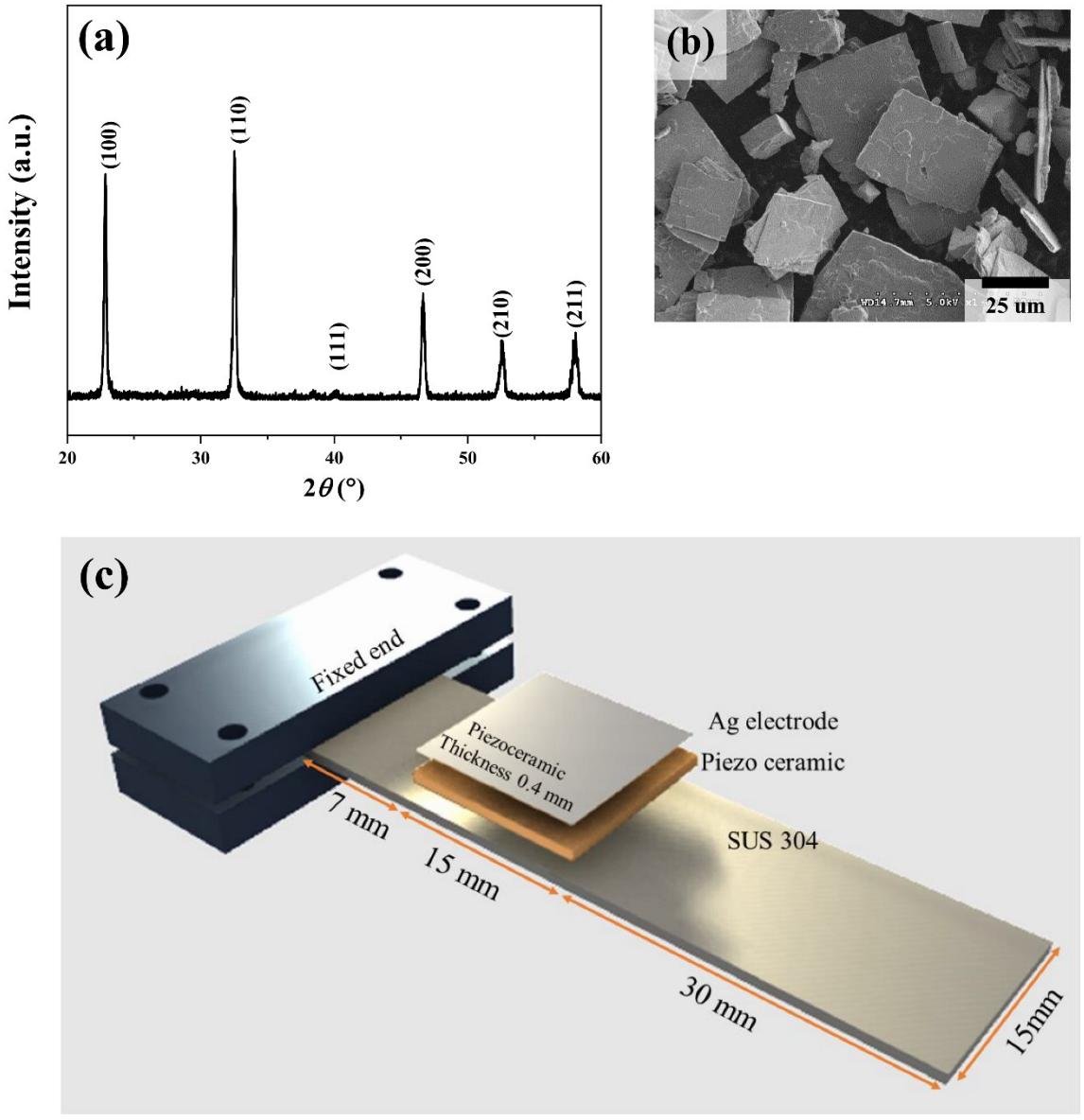

Figure S1. (a) XRD pattern and (b) SEM image of the NNS templates. (c) Schematic of the C-PEH.

2. Various physical properties of the $KN(N_{0.93}S_{0.07})$-BAZ + x mol% CuO piezoceramics

Figures S2(a) and (b) show the XRD patterns of the $KN(N_{0.93}S_{0.07})$-BAZ + x mol% CuO piezoceramics ($0.0 \leq x \leq 3.0$) sintered at 980 °C and 960°C for 10 h, respectively. All samples show the pure perovskite structure without the secondary phase. Relative densities, ε_r, *tan* δ, d_{33} and k_p values of the $KN(N_{0.93}S_{0.07})$-BAZ + x mol% CuO ceramics ($0.0 \leq x \leq 3.0$) at 960 °C for 10 h are provided in Figure S2(b). All the piezoceramics have the low relative densities (< 85% of the theoretical density), indicating that the $KN(N_{0.93}S_{0.07})$-BAZ + x mol% CuO piezoceramics ($0.0 \leq x \leq 3.0$) have not been well densified at 960 °C. Moreover, all the piezoceramics provide low ε_r, d_{33} and k_p values possibly because of their low relative density. These results show that the $KN(N_{0.93}S_{0.07})$-BAZ + x mol% CuO piezoceramics should be sintered at temperatures higher than 960 °C.

The $KN(N_{0.93}S_{0.07})$-BAZ + x mol% CuO piezoceramics ($1.0 \leq x \leq 3.0$) were also sintered at 980 °C for 6 and 13 h, and their relative densities, ε_r, *tan* δ, d_{33}, and k_p values are listed in Table S1. All the piezoceramics exhibited large relative densities (> 94.5% of the theoretical density), indicating that they were well densified at 980 °C for 6 and 13 h. Moreover, they exhibited good dielectric and piezoelectric properties. However, the $KN(N_{0.93}S_{0.07})$-BAZ + x mol% CuO piezoceramics sintered at 980 °C for 10 h show the better dielectric and piezoelectric properties. Therefore, it can be concluded that the $KN(N_{0.93}S_{0.07})$-BAZ + x mol% CuO piezoceramics should be sintered at 980 °C for 10 h.

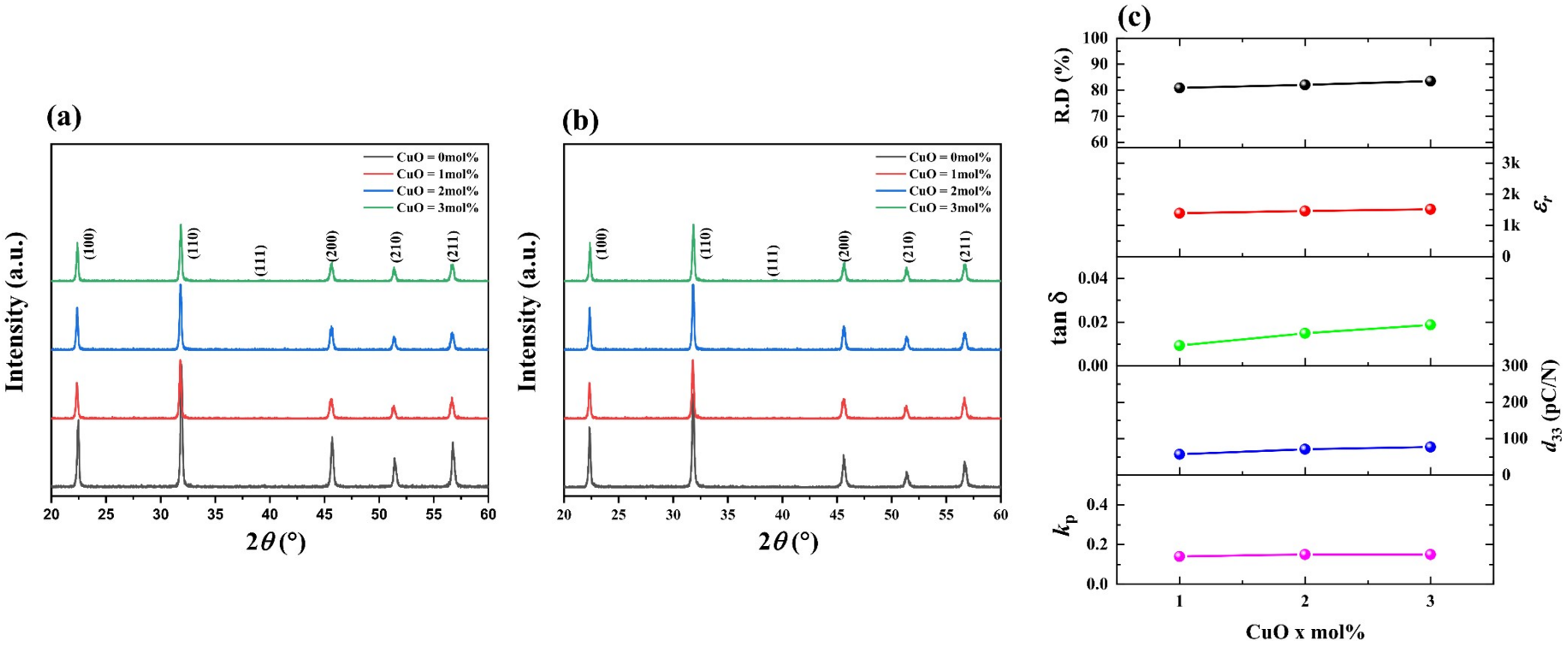

Figure S2. XRD patterns of the KN($N_{0.93}S_{0.07}$)-BAZ + x mol% CuO piezoceramics ($0.0 \leq x \leq 3.0$) sintered at (a) 980 °C and (b) 960 °C for 10h. (c) Relative density, ε_r, *tan δ*, d_{33} and k_p values of the KN($N_{0.93}S_{0.07}$)-BAZ + x mol% CuO piezoceramics ($0.0 \leq x \leq 3.0$) at 960 °C for 10 h.

Table S1. Relative density, ε_r, *tan* δ, d_{33}, and k_p values of the 2.0 mol% CuO-added $KN(N_{0.93}S_{0.07})$-BAZ piezoceramics, which were sintered at 980 °C for 6 and 13 h

Sintering Time	Density(%)	ε_r	tan δ	d_{33} (pC/N)	k_p
6 hours	**95.6**	**2410**	**0.012**	**410**	**0.42**
13 hours	**94.7**	**2318**	**0.014**	**395**	**0.42**

3. ε_r and *tan* δ versus temperature plots and *P-E* hysteresis curves for the CKN($N_{1-z}S_z$)-BAZ piezoceramics

Figures S3(a) and (b) show the ε_r and *tan* δ versus temperature curve for the CKN($N_{1-z}S_z$)-BAZ piezoceramics with z = 0.03 and 0.07. The T_C and T_{T-O} of the piezoceramic (z = 0.03) are 259 and 65 °C, respectively, as displayed in Figure S3(a). T_C was reduced to 189 °C for the sample with z = 0.07, but the variation in T_{T-O} was not significant (Figure S3(b)). The ΔT value of the sample with z = 0.03 is relatively small of 1.0 °C and the increased ΔT value of 7 °C was observed from the sample with z = 0.07. Therefore, sample (z = 0.03) was similar to that of a normal ferroelectric ceramic, and sample (z = 0.07) had relaxor properties.

The *P-E* hysteresis loops of the CKN($N_{1-z}S_z$)-BAZ piezoceramics (z = 0.03 and 0.07) are shown in Figures S3(c) and (d). The saturation polarization (P_{sat}), remnant polarization (P_r) and coercive electric field (E_C) of the CKN($N_{1-z}S_z$)-BAZ piezoceramics are shown in Figure S3(e). The specimen (z = 0.03) provides a normal *P-E* hysteresis loop with relatively large P_{sat}, P_r, and E_C values of 23.5 μC/cm^2, 17.5 μC/cm^2, and 0.95 kV/mm, respectively. A typical *P-E* hysteresis loop was observed from the specimen with z = 0.07 but it showed the reduced P_{sat}, P_r, and E_C values of 20.1 μC/cm^2, 10.1 μC/cm^2, and 0.7 kV/mm, respectively. The decrease in *the* P_{sat} and P_r values could be related to the increase in the amount of *PC* structure, and the decrease in the E_C could be explained by the decrease in the proportion of the *T* phase.

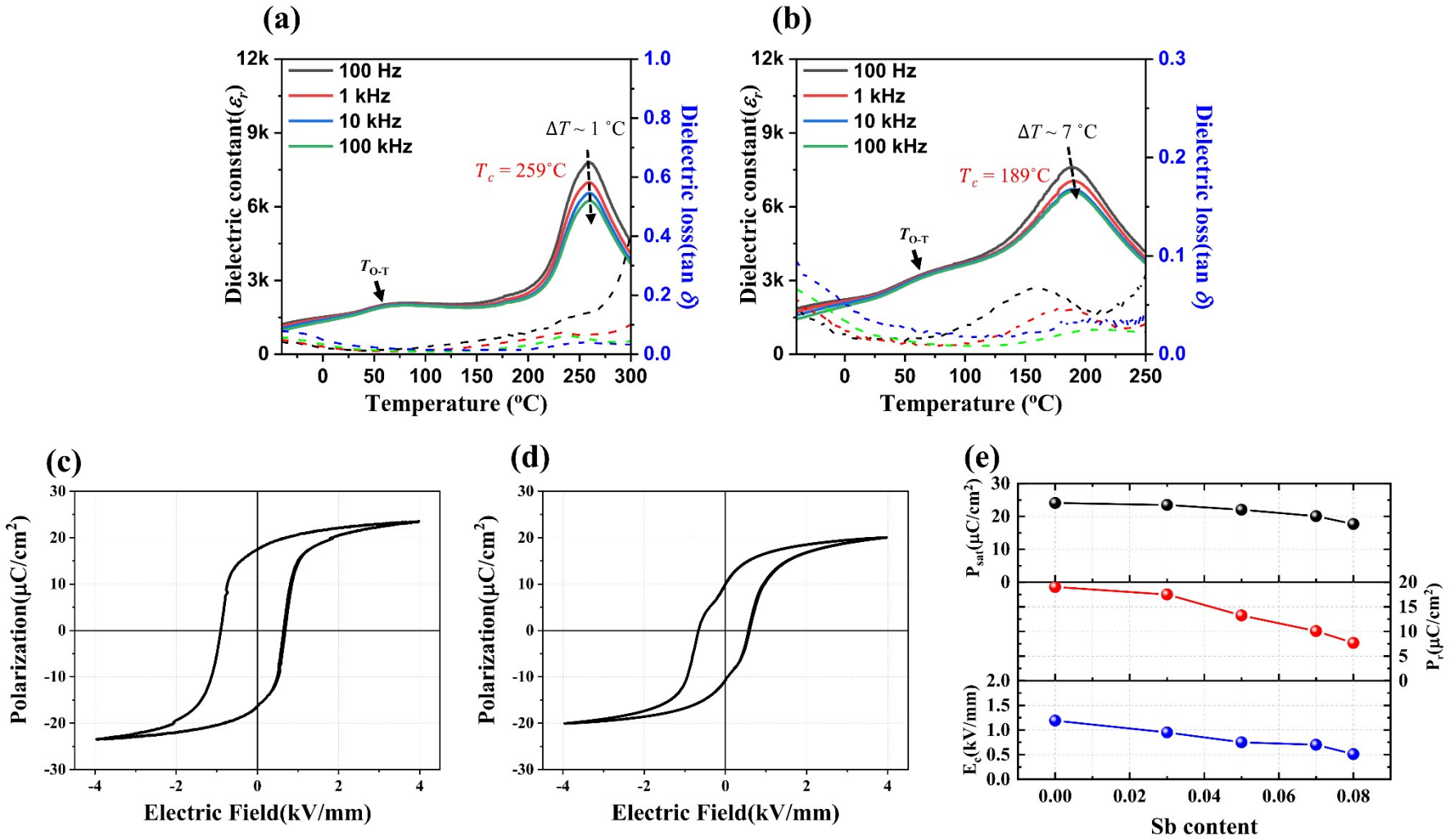

Figure S3. ε_r and *tan* δ versus temperature curve for the CKN($N_{1-z}S_z$)-BAZ piezoceramics with (a) z = 0.03 and (b) 0.07. *P-E* hysteresis loops of the CKN($N_{1-z}S_z$)-BAZ piezoceramics with (c) z = 0.03 and (d) 0.07. (e) P_{sat}, P_r and E_C values of CKN($N_{1-z}S_z$)-BAZ piezoceramics.

4. $1/\varepsilon_r$ versus temperature curves of the CKN($N_{1-z}S_z$)-BAZ piezoceramics

Figure S4(a)–(e) reveal the $1/\varepsilon_r$ versus temperature curves of the CKN($N_{1-z}S_z$)-BAZ piezoceramics with $0.0 \leq z \leq 0.08$. The deviation from the Curie–Weiss law was expressed by $\Delta T_m = T_{dev} - T_m$, where T_m is the transition temperature and T_{dev} is the temperature at which $1/\varepsilon_r$ begins to deviate from the Curie–Weiss law[1, 2]. A normal ferroelectric ceramic has ΔT_m close to zero, while the relaxor ceramic with temperature-independent dielectric properties (or diffuse phase transition) generally exhibited a large ΔT_m[3, 4]. The ΔT_m value of the piezoceramic with z = 0.0 is 0 °C (Figure S4(a)); thus, this piezoceramic has normal ferroelectric properties. The ΔT_m value of the CKN($N_{1-z}S_z$)-BAZ piezoceramics increases with increase in z to 11 °C for the piezoceramic with z = 0.08 (Figures S4(b)–(e)), suggesting that the relaxor properties increased with increasing z.

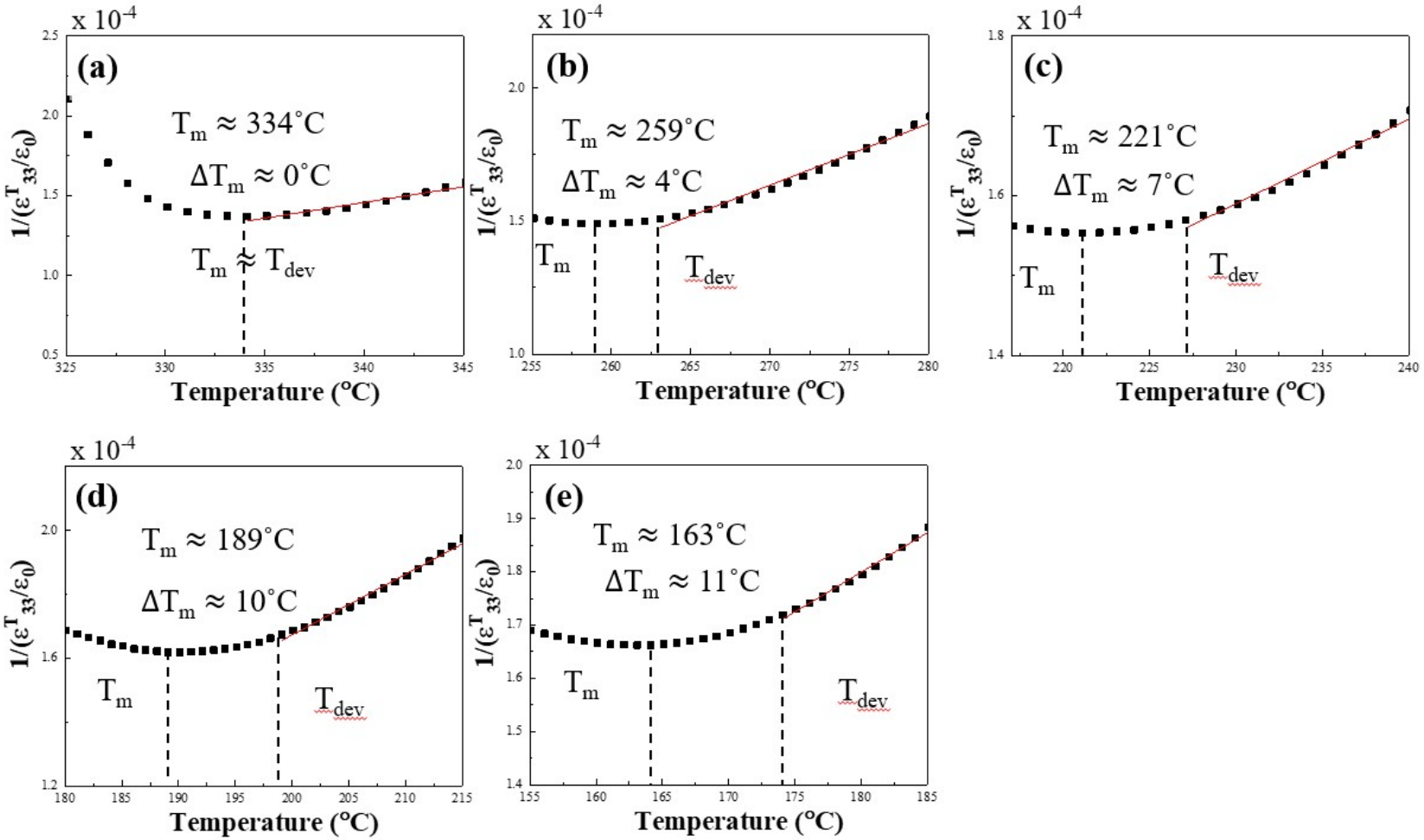

Figure S4. $1/\varepsilon_r$ versus temperature curves of the CKN($N_{1-z}S_z$)-BAZ piezoceramics; (a) z = 0.0, (b) z = 0.03, (c) z = 0.05, (d) z = 0.07, and (e) z = 0.08.

5. ln ($1/\varepsilon_r - 1/\varepsilon_m$) versus ln ($T - T_m$) curves for CKN($N_{1-z}S_z$)-BAZ ceramics

Modified Curie–Weiss law, which is described by $1/\varepsilon_r - 1/\varepsilon_m = (T - T_m)^\gamma/C$, has been also used to investigate the relaxor characteristics of the ceramics. The ε_m is the dielectric constant at T_m, and γ and C are constants[1, 2]. The γ value is virtually 1.0 for the normal ferroelectric ceramic and it is nearly 2.0 for the relaxor ceramics. Figures S5(a)-(e) show the ln ($1/\varepsilon_r - 1/\varepsilon_m$) versus ln ($T - T_m$) curves of the CKN($N_{1-z}S_z$)-BAZ piezoceramics ($0.0 \leq z \leq 0.08$) and the γ value of each piezoceramic is indicated in the corresponding figures. The γ value of the piezoceramic with z = 0.0 is roughly 1.3 that is close to 1.0, confirming that this piezoceramic has the normal ferroelectric properties[3, 4]. The γ value increases with increase in z to approximately 1.7 for the piezoceramic with z = 0.08, as shown in Figure S5(e). Therefore, it can be concluded that the relaxor properties increase with the addition of Sb^{5+} ions to the CKN($N_{1-z}S_z$)-BAZ piezoceramics.

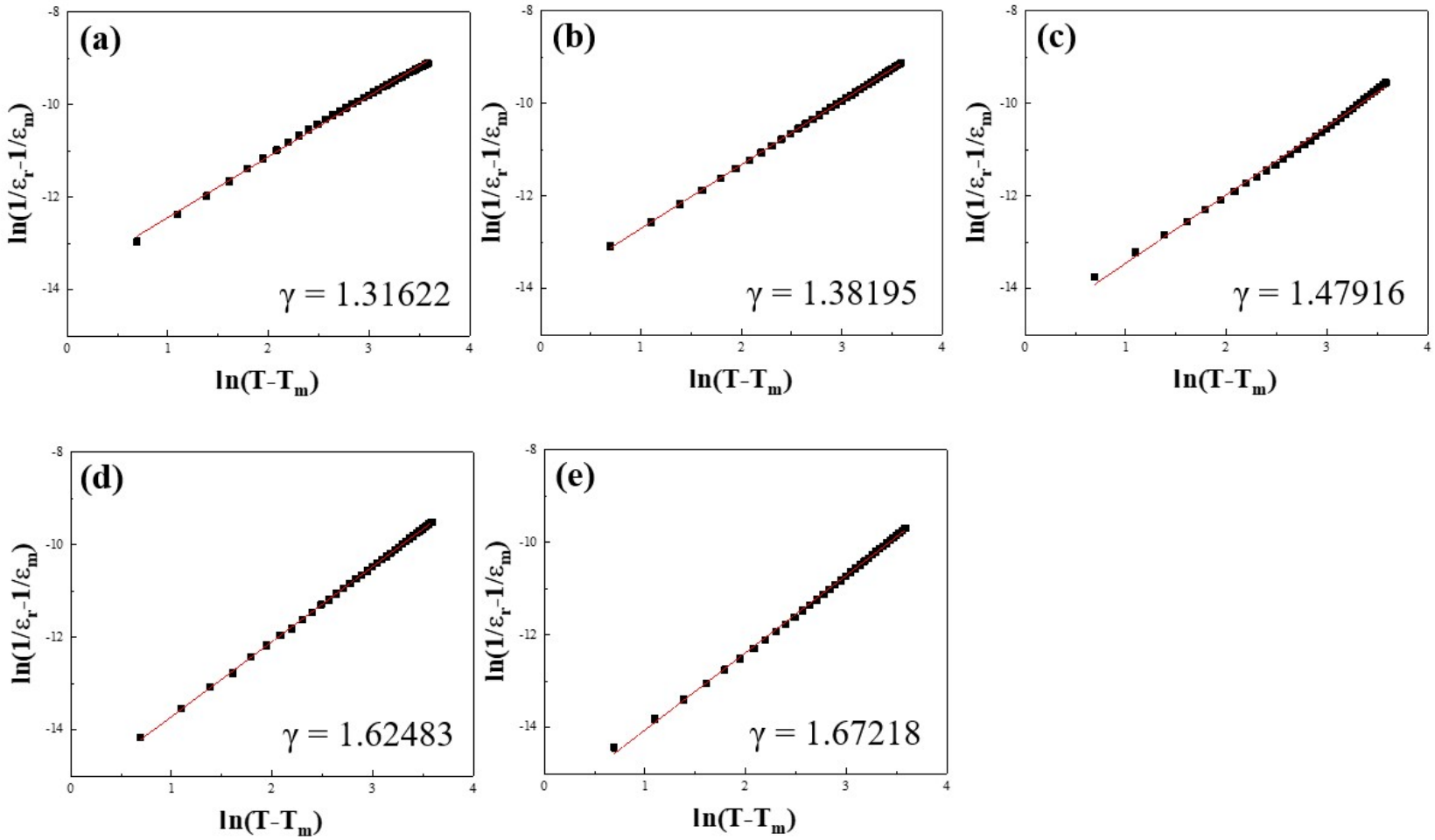

Figure S5. ln ($1/\varepsilon_r - 1/\varepsilon_m$) versus ln ($T - T_m$) curves of the CKN($N_{1-z}S_z$)-BAZ piezoceramics; (a) z = 0.0, (b) z = 0.03, (c) z = 0.05, (d) z = 0.07, and (e) z = 0.08

6. Structural properties of the CKN($N_{0.95}S_{0.05}$)-BAZ piezoceramic textured using NN templates

Figure S6(a) shows an EBSD image of the CKN($N_{0.95}S_{0.05}$)-BAZ piezoceramic textured along the [001] direction using NN templates. Most of the grains were oriented along the [001] direction, as indicated by the red areas. The dark areas may have been defects produced during sample preparation. The (001) pole figure image shows a strong spot at the center of the circle (Figure S6(b)), confirming that most of the grains were oriented along the [001] direction. A SEM image of the CKN($N_{0.95}S_{0.05}$)–BAZ piezoceramic textured along the [001] direction using the NN template is shown in Figure S6(c). Most of the grains were oriented along the [001] direction with the average grain size of approximately 35 μm and thus this piezoceramic is well textured along the [001] direction. However, the holes indicated by arrows were formed inside the grains. The NN templates dissolved during the sintering process, leading to the formation of holes. However, it is difficult to find the holes in the CKN($N_{1-z}S_z$)-BAZ piezoceramics ($0.0 \leq z \leq 0.08$) textured along the [001] direction using the NNS templates (Figures 8(a)-(e)). Therefore, it can be suggested that the NNS templates should be used to texture the CKN($N_{1-z}S_z$)-BAZ piezoceramics to avoid holes.

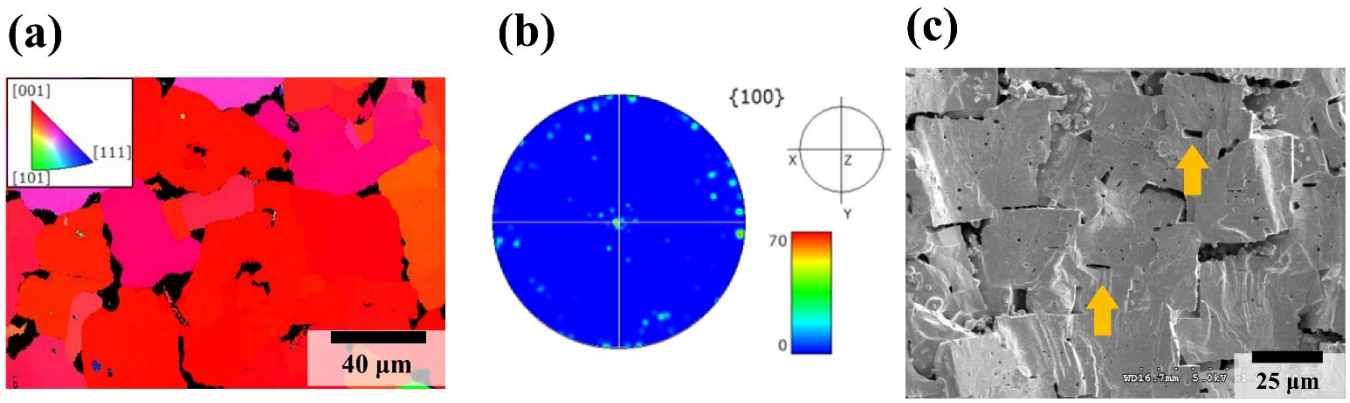

Figure S6. (a) EBSD, (b) (001) pole figure, and (c) SEM images of the CKN($N_{0.95}S_{0.05}$)-BAZ piezoceramic textured along the [001] direction using NN template.

7. ε_r and *tan* δ versus temperature plots and *P-E* hysteresis curves for [001]-textured CKN($N_{1-z}S_z$)-BAZ piezoceramics

Figures S7(a) and (b) provide the change of the ε_r and *tan* δ values with respect to the temperature for the CKN($N_{1-z}S_z$)-BAZ piezoceramics (z = 0.03 and 0.07). The T_C and T_{T-O} of the piezoceramic (z = 0.03) are 253 and 67 °C, respectively, as displayed in Figure 7(a). The T_C reduced to 192 °C for the sample with z = 0.07 but the variation of T_{T-O} is not significant (Figure 7(b)). The ΔT value of the sample with z = 0.03 is 2.0 °C and the enhanced ΔT value of 3.0 °C was detected from the sample (z = 0.07). Therefore, samples (z ≥ 0.03) had relaxor properties.

The *P-E* hysteresis curves of the [001]-textured CKN($N_{1-z}S_z$)-BAZ piezoceramics (z = 0.03 and 0.07) are shown in Figures S7(c) and (d). The P_{sat}, P_r and E_C values of the [001]-textured CKN($N_{1-z}S_z$)-BAZ piezoceramics are shown in Figure S7(e). A typical *P-E* hysteresis loop was observed from the specimen (z = 0.03) and it provides relatively large P_{sat}, P_r, and E_C values of 19.6 μC/cm^2, 15.3 μC/cm^2, and 0.94 kV/mm, respectively. The sample (z = 0.07) also shows a normal *P-E* hysteresis loop but it provided the decreased P_{sat} (12.6 μC/cm^2) P_r (7.1 μC/cm^2), and E_C (0.55 kV/mm) values. The decrease in P_{sat} and P_r values can be explained by the increased proportion of the *PC* structure, and the reduction in E_C is attributed to the decrease in the proportion of the *T* phase.

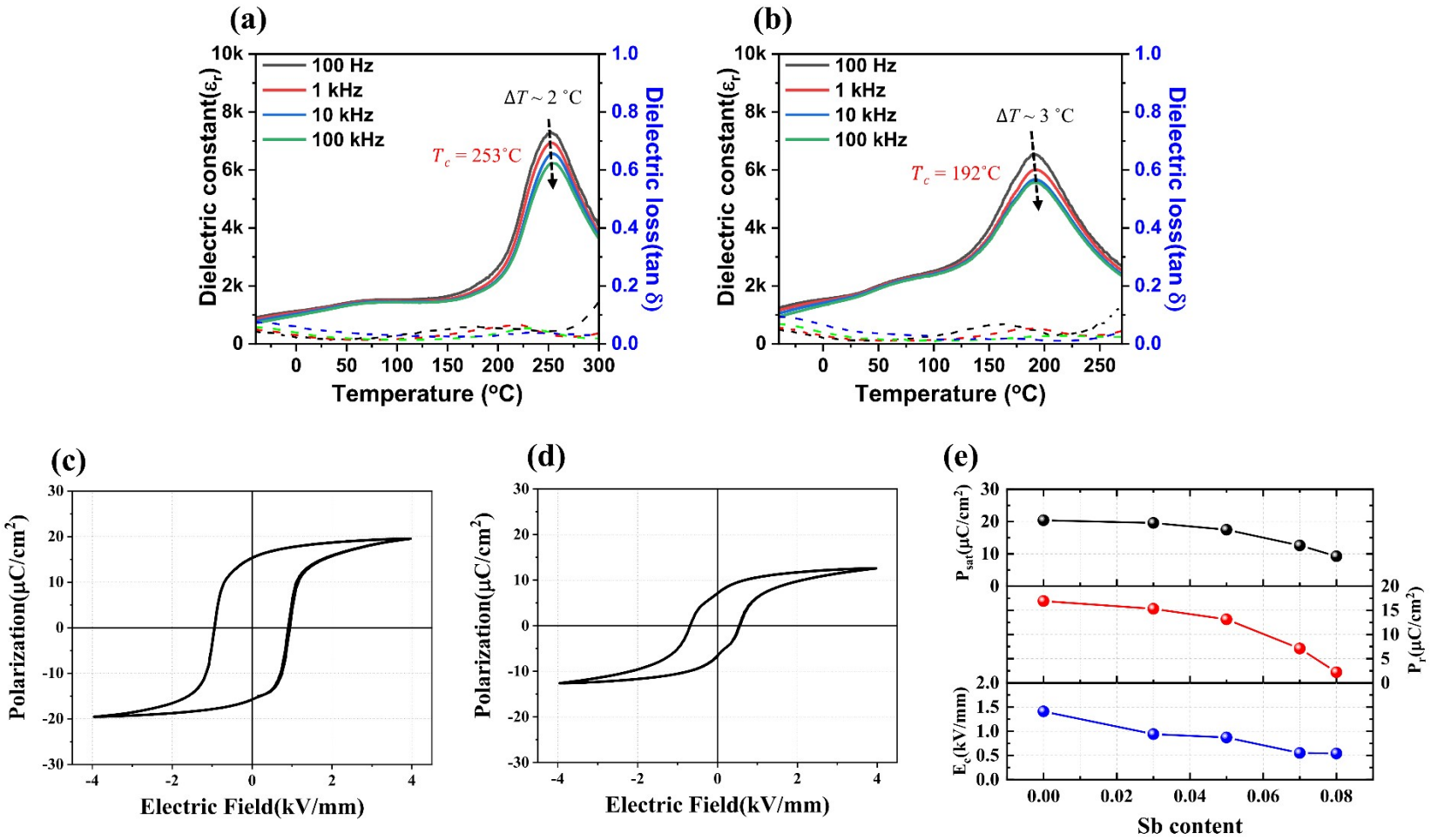

Figure S7. ε_r and *tan* δ versus temperature curve for the [001]-textured CKN($N_{1-z}S_z$)-BAZ piezoceramics with (a) z = 0.03 and (b) 0.07. *P-E* hysteresis loops of [001]-textured CKN($N_{1-z}S_z$)-BAZ piezoceramics with (c) z = 0.03 and (d) 0.07. (e) P_{sat}, P_r, and E_C values of the [001]-textured CKN($N_{1-z}S_z$)-BAZ piezoceramics.

References

1. K. Uchino and S. Nomura, *Ferroelectrics*, 1982, **44**, 55–61.
2. S. W. Kim, T. G. Lee, D. H. Kim, E. J. Kim, D. S. Kim, W. S. Kang, W. Jo, S. J. Lee, S. H. Han and H. W. Kang, *J. Am. Ceram. Soc.*, 2019, **102**, 6837–6849.
3. T. A. Duong, F. Erkinov, M. Aripova, C. W. Ahn, B. W. Kim, H. S. Han and J. S. Lee, *Ceram. Int.*, 2021, **47**, 4925–4932.
4. S. -J. Chae, S. -J. Park, I. -S. Kim, S. Kwak, H. Ryu and S. Nahm, *J. Eur. Ceram. Soc.*, 2024, **44**, 3926–3936.